

Effects of flow constriction on foamed viscous shear-thinning fluids downstream of a continuous multi rotor-stator foaming device

Jabarkhyl, Saifullah; Zhu, Shiping; Barigou, Mostafa

DOI:

<https://doi.org/10.1016/j.jfoodeng.2020.110341>

Citation for published version (Harvard):

Jabarkhyl, S, Zhu, S & Barigou, M 2020, 'Effects of flow constriction on foamed viscous shear-thinning fluids downstream of a continuous multi rotor-stator foaming device', *Journal of Food Engineering*, vol. 292, 110341. <https://doi.org/10.1016/j.jfoodeng.2020.110341>

[Link to publication on Research at Birmingham portal](#)

General rights

Unless a licence is specified above, all rights (including copyright and moral rights) in this document are retained by the authors and/or the copyright holders. The express permission of the copyright holder must be obtained for any use of this material other than for purposes permitted by law.

- Users may freely distribute the URL that is used to identify this publication.
- Users may download and/or print one copy of the publication from the University of Birmingham research portal for the purpose of private study or non-commercial research.
- User may use extracts from the document in line with the concept of 'fair dealing' under the Copyright, Designs and Patents Act 1988 (?)
- Users may not further distribute the material nor use it for the purposes of commercial gain.

Where a licence is displayed above, please note the terms and conditions of the licence govern your use of this document.

When citing, please reference the published version.

Take down policy

While the University of Birmingham exercises care and attention in making items available there are rare occasions when an item has been uploaded in error or has been deemed to be commercially or otherwise sensitive.

If you believe that this is the case for this document, please contact UBIRA@lists.bham.ac.uk providing details and we will remove access to the work immediately and investigate.

Effects of flow constriction on foamed viscous shear-thinning fluids downstream of a continuous multi rotor-stator foaming device

Saifullah Jabarkhyl¹, Shiping Zhu², Mostafa Barigou^{1*}

¹School of Chemical Engineering, University of Birmingham, Edgbaston, Birmingham B15 2TT, UK

²Unilever R&D Refreshment Discovery, Colworth Science Park, Sharnbrook, MK44 1LQ, UK

Abstract

Foam flow through processing equipment can seriously affect the structure of the foam and its quality attributes. In the design of a foam formulation and its flow system, it is therefore important to consider the possible implications on the end-of-pipe structure of the foam to ensure preservation of product quality. We study the flow through a straight pipe with and without the presence of a narrow orifice plate and, hence, the dynamic stability of wet food relevant foams of fine texture and high static stability generated from complex formulations of viscous shear-thinning fluids in a continuous multi rotor-stator device. The effects of fluid formulation, gas-liquid ratio, rotor speed and constriction aperture size are investigated. Constricted foam flow can cause important transformations in the foam due to significant bubble coalescence and loss of air volume resulting in much coarser and much less stable foam. Increased surfactant content, liquid viscosity and rotor speed reduce bubble coalescence and help preserve foam structure.

Keywords: foam flow; flow constriction; foam dynamic stability; pressure drop; wet foam; non-Newtonian liquid.

* Corresponding author; email: m.barigou@bham.ac.uk

1. Introduction

Foams are complex multi-component structures which enjoy many applications in a wide range of industries including food, pharmaceuticals, mineral transport, oil and gas. Dry foams are structured two-phase fluids in which polyhedral gas bubbles are separated by interconnecting thin liquid films and Plateau borders which denote the regions of intersection of the thin films, whilst wet foams including food foams tend to be bubbly liquids with round bubbles. Foams represent an important class of structured fluids possessing a complex rheology and flow behaviour strongly dependent upon local structure and chemical composition. The nature of the foam, i.e. its texture and stability, and its overall rheological and flow properties can determine both the economic and technical successes of the industrial process concerned. For example, some aerated products possessing a smaller bubble size and a uniform bubble size distribution have a much longer shelf-life and better consumer perception because of their better creaminess (Müller-Fischer and Windhab, 2005, Müller-Fischer, Suppiger and Windhab, 2007b). Information on both the static as well as dynamic behaviour of foams is of direct value to the manufacture of a wide range of foods. Foam flow through processing equipment usually affects the structure of the foam and its properties. In the design of a food foam formulation and its flow system, it is therefore important to consider the possible effects on the end-of-pipe structure and, hence, quality attributes of the foam. These effects may have serious practical implications and have to be carefully considered as preservation of product structure and quality during processing is important.

Effective stabilisation of a food foam is critical since bubble coalescence can lead to a loss of microstructure and hence a deterioration of foam organoleptic properties such as texture and taste. Food foams are often stabilised with protein molecules (β -lactoglobulin, casein, albumin and whey protein isolate) commonly derived from milk and egg (Zayas, 1997). Protein molecules drastically alter the interfacial rheological properties providing a strong mechanical barrier against bubble coalescence (Murray *et al.*, 2006). More recently, however, non-ionic surfactants such as polyglycerol fatty acid ester, PGE 55, hydrophobins and food-grade particles (agar gel particles) have attracted considerable attention (Curschellas *et al.*, 2013, Cox, Aldred and Russell, 2009, Ellis *et al.*, 2017, Dickinson, 2010), as they have been shown to have excellent foam stabilisation properties (Duerr-Auster *et al.*, 2007, Duerr-Auster *et al.*, 2008, Curschellas *et al.*, 2013b). The irreversible adsorption of PGE 55, once exposed to heat above its Kraft temperature (58 °C), can significantly reduce the rate of coalescence. In addition, the presence of multilamellar vesicles, formed as a result of its very low critical aggregation concentration (cac), in films and Plateau borders greatly improves stabilisation against drainage (Curschellas *et al.*, 2013). Likewise, the addition of food hydrocolloids such as guar gum, xanthan gum and low-molecular weight viscosity-enhancing sucrose can drastically reduce foam drainage. Inclusion of hydrocolloids tends to also improve foam texture and smoothness in products such as ice cream (Murray *et al.*, 2006). In the case of proteins, inclusion of these viscosity modifying ingredients may lead to synergistic interaction, however, but this is not the case with PGE 55.

74

75 Any process where significant deformation of the air-water interface is likely to occur may lead to
76 bubble coalescence. Such processes include the flow of aerated products through nozzles, pipes, pipe
77 fittings and pumps. In addition, in the food industry, aeration is predominantly performed under
78 pressurised conditions (typically, 2–3 bar) to reduce the effective air volume fraction inside the mixing-
79 head chamber of the foam generator and, hence, diminish the probability of bubble collision and
80 re-coalescence during foam generation. Once the foam is discharged to atmosphere, bubbles expand as
81 a result of the pressure drop, but an over-beating phenomenon can take place as a result of increased
82 residence time because of the reduced gas volume fraction inside the mixing-head chamber.

83

84 Operations involving rapid pressure drop (e.g. flow from a nozzle), steady and elongation shear (e.g.
85 flow through a pipe) can lead to a severe loss of foam attributes. Much of the current understanding of
86 these effects stems from the engineering literature. Calvert and co-workers were the first to examine the
87 effects of geometric constrictions (commercial diaphragm, globe and ball valves) on fire-fighting
88 foams. It was found that a flow constriction (globe valve) with an intricate flow path (high shear rates)
89 and a high residence time led to foam breakdown in contrast to a diaphragm or ball valve (Calvert and
90 Nezhati, 1987, Calvert, 1988). Deshpande and Barigou (2000, 2001a, 2001b) examined the flow of dry
91 and wet detergent-stabilised foams in straight pipes fitted with a variety of flow constrictions
92 (expansion, contraction, orifice plate, perforated plate, bend, elbow). They found that foam flow
93 through pipe fittings is characterised by complex phenomena which influence foam structure, liquid
94 holdup and flow regime. In general, the liquid holdup decreases substantially downstream of a fitting,
95 which results in intense recirculation flow patterns upstream and a much drier foam downstream. A
96 sudden expansion can lead to a complete breakdown of the foam (Deshpande and Barigou, 2001a).
97 Thus, pipe fittings can have serious effects on the end-of-pipe structure of a foam, hence, resulting in
98 important practical implications for the preservation of product structure. Similar but more detailed
99 work has been recently reported on the flow of monolayer foams through narrow 2D channels with
100 constrictions (Badve and Barigou, 2020). However, little is known about the flow behaviour of food
101 foams which have a more complex composition and, thus, a more complex rheology.

102

103 Dickinson and coworkers developed an apparatus for the direct visualisation of foam microstructure
104 under rapid pressure drop. One major finding from their study was that foam made from gelatine was
105 less likely to undergo coalescence when exposed to rapid pressure drop (Dickinson *et al.*, 2002, Murray
106 *et al.*, 2006). Similarly, Heuer *et al.* (2007) reported the effects observed on the microstructure of a
107 model food foam, using a Linkam pressure cell to pressurise the foam to different levels from
108 atmospheric pressure up to 11 bar and then releasing the pressure at varying rates. The setup was also
109 used to study the effects of disproportionation and single and multiple pressure cycles on the resultant
110 foam. Significant pressure drops were quite destructive, with most coalescence observed from 2 bar

down to 1 bar absolute. Surprisingly, however, no coalescence was observed from 11 bar, the starting pressure, down to 2 bar absolute. Significant effects were seen when the pressure release rates were varied. Slow pressure release rates (2 min per bar released) had the effect of causing increased coalescence events, when compared to very quick release rates (Heuer *et al.*, 2007). Other studies on continuous foaming of Newtonian and non-Newtonian model liquid food formulations using a rotor-stator device all agree on the fact that an increase in rotor speed leads to a significant reduction in bubble size (Müller-Fischer, Suppiger and Windhab, 2007b, Jabarkhyl *et al.*, 2020a, Mary *et al.*, 2013). However, there are conflicting reports on the effects of static pressure and residence time which hitherto remain unclear and hence need further investigation (Mary *et al.*, 2013, Balerin *et al.*, 2007, Müller-Fischer and Windhab, 2005)

Recently, we investigated the continuous foaming of viscous non-Newtonian shear-thinning model food liquids in a pilot-scale multi rotor-stator high-shear device (Jabarkhyl *et al.*, 2020a), and studied the effects of processing parameters including rotor speed, gas-liquid ratio, surfactant and xanthan gum concentration. Furthermore, we studied the steady-shear as well as viscoelastic rheological properties of the various wet foams thus generated (Jabarkhyl *et al.*, 2020b). The foams exhibited high static stability and resistance to steady shear with no bubble breakage observed when the foams were sheared between parallel-plates on a rheometer. In this paper, we study the flow of these wet model food foams and their dynamic stability as they flow through a straight pipe and interact with a narrow orifice plate constriction. Narrow orifices of different aperture sizes are used to generate significant pressure drops on a lab scale which would mimic the flow of such foams through nozzles and pipe fittings in industrial setups. The effects of fluid formulation, gas-liquid ratio, rotor speed and orifice aperture size, are investigated.

2. Materials and methods

2.1 Model fluids and foam generation

The materials and methods used are based on our recent related work which studied the continuous production of foams from complex viscous shear-thinning fluids in a multi rotor-stator device and their rheological properties (Jabarkhyl *et al.*, 2020a, Jabarkhyl *et al.*, 2020b). We used five model complex non-Newtonian fluid formulations of shear-thinning rheology consisting of a mixture of polyglycerol fatty acid ester (PGE 55), xanthan gum (XG), caster sugar and sodium azide, denoted MF1, MF2, MF3, MF4 and MF5, whose composition and physical properties are summarised in Table 1. Foams were generated by aerating the model fluids in a pilot-scale continuous multi rotor-stator unit (Megatron FM 12- 50/2 HR) depicted in Fig. 1. The geometrical dimensions of the 12 rotor-stator pairs positioned in series inside the foam generator are provided in Table 2. A Julabo F-25 cooling system enabled the foam temperature at the outlet of the foaming unit to be kept approximately equal to the inlet feed temperature (20 °C). Foams of different textures were obtained by using combinations of liquid and air flowrates within the range 2.5 – 5.0 L h⁻¹ and 0.1 – 12.5 L hr⁻¹, respectively. Further details of the

protocols adopted for the preparation of the model fluids and foams can be found in our previous work (Jabarkhyl *et al.*, 2020a, Jabarkhyl *et al.*, 2020b).

2.2 Foam characterisation

The foams produced were characterised by determining their air volume fraction, their bubble size distribution and their rheological properties.

2.2.1 Air volume fraction

The foam air fraction (ϕ_e) was experimentally determined by collecting foam samples of known volume at the outlet of the foam generator and measuring the mass of liquid within. The foaming process aims to maximise ϕ_e and achieve the maximum theoretical value $\phi_{th}^{(P)}$, defined in terms of the pressure-dependent volumetric air flowrate $Q_G^{(P)}$ and liquid volumetric flowrate Q_L , as:

$$\phi_{th}^{(P)} = \frac{Q_G^{(P)}}{Q_G^{(P)} + Q_L} \quad (1)$$

The effects of pressure are taken into account through the ideal gas law, thus:

$$F_E = \phi_{th}^{(P_{atm})} \left(\frac{P_{atm}}{P} \right) \quad (2)$$

where F_E is the foam expansion ratio dependent on pressure, air and liquid flowrate in the mixing-head chamber and $\phi_{th}^{(P_{atm})}$ is the equivalent air volume fraction at atmospheric pressure P_{atm} .

Another important parameter is the average residence time, τ , inside the mixing-head chamber of the foam generator (Fig. 1) which can be estimated using the foam volumetric flowrate (V_{foam}) and the volume of the mixing-head chamber ($V = 85$ mL), thus:

$$\tau = \frac{V}{V_{foam}} = \frac{V}{Q_L + Q_G^{(P)}} \quad (3)$$

2.2.2 Foam bubble size distribution

A foam sample of about 5 ml was carefully placed inside a plastic drinking straw using a pipette and sealed prior to scanning. X-ray micro-Computed Tomography measurements were performed on a Skyscan instrument (Skyscan 1172, Bruker, Belgium) operating at a source voltage of 80 kV and current of 98 μ A, with an image resolution of $3.78 \mu\text{m pixel}^{-1} \times 5.78 \mu\text{m pixel}^{-1}$. No filter was used since foam has a low density and a low attenuation coefficient. Each sample was scanned over 180 degrees in

discrete steps of 0.4 degree with a frame averaging of 4 to acquire up to 1200 radiographic images of 1048×2000 pixels. The scan duration was limited to less than 20 min to avoid any significant effects arising from gravity drainage of the foam. A computer recorded the images for subsequent reconstruction using NRecon software (Bruker micro-CT, Belgium), based on the principle of filtered back-projection utilising the method of cone-beam reconstruction. At least three samples of the same foam were scanned to obtain statistically significant results. Depending on the scanning parameters implemented, the reconstruction procedure took approximately 5 – 10 min. Finally, the projection images were uploaded to a CTan software (Bruker micro-CT, Belgium) for detailed image analysis. The technique provides non-invasively a high-resolution 3D model of the microstructure of a stable foam, from which the bubble size distribution and various descriptive statistics are derived including the Sauter mean bubble diameter (D_{32}) defined as:

$$D_{32} = \frac{\sum n_i d_i^3}{\sum n_i d_i^2} \quad (4)$$

where n is the number of bubbles of diameter d in class size i . The technique and its protocol have been described in more detail in our previous works (Lim and Barigou, 2004, Barigou and Douaire, 2013, Jabarkhyl *et al.*, 2020a).

2.2.3 Rheological properties of model fluids and foams

The oscillatory rheology of the foams studied was characterised at 25 °C using a 40 mm parallel-plate geometry with a gap of 2.0 mm fitted on a controlled stress/strain rheometer (Discovery HR-2, Hybrid Rheometer, TA, USA). Amplitude sweep tests with % strain varying in the range 0.01 to 1000% were conducted at 1 Hz frequency to determine the viscoelastic moduli (G' , G''). The use of roughened plates (58 µm equivalent grit size) enabled the elimination of slip. Measurements were repeated at least three times using fresh samples and an average obtained. The measurement time was kept short to avoid foam drainage effects. More details on the rheometry procedures adopted can be found in our previous work (Jabarkhyl *et al.*, 2020b).

2.3 Foam flow through an orifice constriction

The foam flow rig consisted of two lengths of acrylic pipe of 30 mm diameter and 0.5 m length connected by bolted flanges, as schematically represented in Fig. 2. Digital pressure transducers (Druck, UK) connected to a computer via a data logger (PicoLog 1000 Series), were installed along the flow pipe including at the inlet and at the exit of the constriction for pressure drop measurements. A thin stainless-steel orifice plate (1.5 mm thick) was inserted between the two flanges to act as a constriction to the foam flow. The orifice sizes investigated were: $D_o = 0.4, 0.5, 0.6, 0.8$ and 1.8 mm

diameter corresponding, respectively, to orifice-pipe area ratios of $A_o/A = 0.00020$; 0.00032 ; 0.00046 ; 0.00082 ; 0.00413). A foam sampling point was fitted at the exit of the constriction.

In a typical experiment, foam generated by the continuous rotor-stator device is fed directly into the flow pipe. Foam samples are collected at the exit of the constriction for off-line analysis using an X-ray micro-CT technique to determine the bubble size distribution. At this point, the foam pressure would have dropped to nearly atmospheric and sampling at the wall does not introduce any significant effects on the foam microstructure. Upstream of the constriction, however, the foam pressure is high and wall sampling would cause expansion of the foam. Hence, the foam is photographed in-situ at the pipe wall using a digital camera fitted onto a Leica microscope with a variable zoom lens, and the bubble size distribution determined via image analysis using ImageJ software. Typically, a sample of at least 500 bubbles is used and only bubbles in the centre of an image are analysed to avoid curvature effects. It should be pointed out, however, that imaging at the wall does not yield accurate information on the full 3D microstructure of the foam and is only used as a rough indication of the bubble size when other means of visualisation are not possible (Deshpande and Barigou, 2000, Deshpande and Barigou, 2001a, Deshpande and Barigou, 2001b). Before taking measurements, the foam is allowed to flow through the constricted pipe for up to 20 min until steady state conditions are reached, i.e. when pressure readings and volume fraction of the foam collected at the exit of the pipe stabilise.

2.4 Foam static stability

Foam static stability was determined by monitoring, at a constant temperature of 50°C over a period of several weeks, liquid drainage in 50 mL samples collected at relevant points of the flow system. Thus, transients of drained liquid were obtained for all experimental conditions investigated. In each case, three samples were analysed and an average obtained.

2.5 Statistical analysis

All measurements were performed in triplicate. A one-way analysis of variance (ANOVA) was conducted using the well-known Minitab statistical software, and a Tukey's pairwise comparison test was performed to find statistically significant results (i.e. $p < 0.05$). Results are reported as mean values \pm standard deviation in Tables 3 – 6.

3. Results and discussion

3.1 Aeration efficiency

Aeration efficiency ($\eta = \phi_e/\phi_{th}$) is an important feature of the foam generation process which indicates the ability to incorporate all of the available gas into the foaming liquid to make a homogeneous foam. Thus, optimum aeration is achieved when the theoretical and experimental values of volume gas

fraction are equal (Eq. (1)). At atmospheric pressure, i.e. when the foam flow rig is not connected to the rotor-stator device and the generated foam is simply discharged to atmosphere, maximum aeration efficiency was achieved for all model fluids at most rotor speeds when the G/L ratio (ratio of air to liquid volumetric flowrate) was set to 1.0, 1.5 and 2.0, corresponding respectively to $\phi_{th}^{(Patm)} = 0.50, 0.60$ and 0.67 . These conditions were also achieved when the foam flow rig was connected to the foam generator unit and flow took place through the short straight pipe without a constriction; in this case the pressure inside the mixing-head chamber was close to atmospheric given that the linear pressure drop in the pipe was small (~ 0.1 bar), as shown in Table 3. Such a low pressure drop along the pipe did not have any significant effects on the microstructure of the flowing foam including bubble size and gas holdup.

In the presence of a flow constriction, maximum aeration efficiency was only achieved when the pressure drop ΔP_c across the constriction was below 1.0 bar, independent of the G/L ratio used (Table 3). The reduction in aeration efficiency with increasing pressure drop may be attributed to the relatively large increase in bubble size across the constriction caused by bubble coalescence - note that bubble expansion through the constriction accounts for only a relatively small part ($\sim 20\%$) of this increase in bubble size.

3.2 Effects of processing parameters on bubble size distribution

3.2.1 Effects of residence time

Whilst it is well known that increasing the rotor speed reduces bubble size (Jabarkhyl *et al.*, 2020a, Mary *et al.*, 2013, Müller-Fischer, Suppiger and Windhab, 2007b), the effects of residence time and G/L ratio are not always clearly identified. For example, Muller-Fischer, Suppiger & Windhab (2007b) reported that a longer residence time led to a smaller bubble size, whereas Mary *et al.* did not observe a clear trend. Such conflicting reports may be due to differences in foaming solutions (Newtonian, non-Newtonian), processing parameters and hydrodynamic conditions (rotor speed, pressure and G/L ratio, laminar flow, turbulent flow), imaging procedures (online, off-line) and different rotor-stator geometries; in addition, the cross-influence of residence time and dispersion viscosity is not taken into account in most cases (Müller-Fischer, Suppiger and Windhab, 2007b, Mary *et al.*, 2013).

In this study, for a fixed G/L ratio, doubling the residence time led to a significant reduction in bubble size, as shown in Fig. 3, the extent of reduction being a function of G/L ratio and N . The smaller the G/L ratio, the greater the influence of residence time on the bubble size distribution (BSD) and, hence, on D_{32} . Increasing the G/L ratio (i.e. increasing ϕ_e) and τ leads to a narrower, more uniform BSD; the effects of τ reduce as the G/L ratio and N increase. These observations can be explained in terms of bubble breakage and coalescence frequency inside the mixing-head chamber. At smaller G/L ratios,

the probability of bubble coalescence is low and bubble breakage is predominant and, hence, a longer residence time results in a smaller bubble size. At higher G/L ratios, the larger bubble number density leads to an equilibrium between bubble breakage and coalescence, which reduces the effect of τ . Under all conditions, the effect of τ diminishes with increasing N . It should also be pointed out that substantial variations in τ are required to generate any noticeable effects on bubble size.

3.2.2 Effects of air volume fraction

Typical results depicting the effects of air volume fraction on bubble size for a fixed residence time ($\tau = 40$ s) are shown in Fig. 4. The BSD is more or less the same for $G/L \leq 1.0$, however, the BSD becomes much narrower and more uniform for $G/L \geq 1.5$. The data fall into two distinct regions: (i) a region of constant D_{32} corresponding to low and medium ϕ_e values; and (ii) a region of sharp decline in D_{32} at higher gas volume fractions. Müller-Fischer, Suppiger and Windhab (2007b) using a similar rotor-stator device, but a different non-Newtonian fluid formulation and operating at much higher rotor speeds and a much shorter residence time, reported the same plateau region beyond which, however, D_{32} increases sharply as a function of ϕ_e . The rise in bubble size was attributed to the increased coalescence rate because of the higher rotor speeds and the higher ϕ_e values they used as well as the significant time lag between foam sampling and bubble size measurement using a light microscope (Müller-Fischer, Suppiger and Windhab, 2007b). The latter effect was obviated here because of the high stability of the foams (Jabarkhyl *et al.*, 2020a) and the use of fast X-ray micro-CT analysis. There is no significant effect on BSD for $G/L < 1.0$, however, the BSD becomes much more uniform for $G/L \geq 1.5$.

3.3 Foam flow through a short straight pipe

Initial foam flow experiments were conducted through a short straight pipe without constriction. Using foams generated from the different model fluids (Table 1), varying the foam flowrate in the range 7.5 – 16.0 L hr⁻¹ by varying the G/L ratio from 0.5 to 2.0, engendered a maximum pressure drop along the pipe of about 0.1 bar. Such a pressure drop was too low to cause any significant effects on the foam microstructure and texture along the pipe. These foams exhibit high static and quasi-static stability (Jabarkhyl *et al.*, 2020a).

3.4 Foam flow through a straight pipe with an orifice constriction

3.4.1 Effects of G/L ratio

The diameter of the orifice constriction was varied in the range 0.5 – 1.8 mm to achieve different pressure drops in the foam flow (Table 3). X-ray micro-CT images showing the microstructure of foams generated from MF2 flowing with and without a flow constriction are depicted in Fig. 5a. In the absence of a flow constriction, the foams exhibit a fine texture characterised by a narrow BSD with a peak at 100 μ m and the vast majority of bubbles being less than 200 μ m. In contrast, in the presence of a flow

constriction the BSD is much wider and the foam texture much coarser with bubble sizes up to 600 μm being observed. Though the relative frequency of the larger bubbles is small, they do contribute significantly to the Sauter mean diameter, as shown in Fig. 6.

Over the range of conditions investigated, the mean bubble size measured at the exit of the constriction increased approximately linearly as a function of ΔP_c , as shown in Fig. 6. In a short straight pipe (data points corresponding to approximately zero pressure drop), the G/L ratio has a relatively small effect on D_{32} . Upstream of the constriction, the mean bubble size is independent, within experimental error, of the orifice size used, as revealed by the data presented in Table 3. A reduction in orifice size corresponds to an increase in pressure inside the mixing-head chamber, the effect of which seems to be cancelled by a longer residence time leading to a constant mean bubble size. An identical maximum bubble size is expected, provided the air volume fraction and the residence time are kept constant inside the mixing-head chamber, independent of the applied static pressure, since the critical Weber number is independent of pressure (Müller-Fischer, Suppiger and Windhab, 2007b).

A higher G/L ratio, i.e. a higher gas holdup, causes a significantly larger increase in D_{32} , reflected in a greater slope of the linear trend. Qualitatively similar findings were reported by Müller-Fischer and coworkers for different foam formulations and flow conditions (Müller-Fischer, Suppiger and Windhab, 2007b, Müller-Fischer and Windhab, 2005). The results appear to suggest that at low pressure drops, the foam is able to squeeze through the constriction without incurring significant structural damage. As ΔP_c increases, the foam texture becomes coarser due to increased bubble coalescence. This effect seems to be even more significant for dryer foams probably because of the higher bubble density and thinner liquid films. To illustrate the severity of the foam degradation that can occur, flow experiments were conducted through an even narrower 0.4 mm orifice creating a much higher pressure drop of 2.5 bar, and the results are depicted in Fig. 7. The BSD becomes much wider and positively skewed. In this case, there was an almost 5 fold increase in the D_{32} from ~ 130 to ~ 600 μm .

These results serve to demonstrate that even such statically highly stable foams, do incur significant structural transformations as a result of dynamic interactions with processing equipment. Hence, the transport and processing of these structured fluids should avoid high pressure drops and should be conducted as far as possible under conditions of pressure close to atmospheric.

3.4.2 Effects of PGE 55 surfactant concentration

Flow experiments were conducted through a short straight pipe first without and then with a constriction (0.8 mm orifice plate) at G/L = 1.5, using foams generated from fluids MF1, MF2 and MF3 containing respectively, 0.2, 0.5 and 1.0 wt% PGE 55 surfactant, but the same XG concentration (0.5 wt%). It should be pointed out that the cac (critical aggregation concentration) of PGE 55 is very low (0.00001

wt%), such that the concentrations used here are orders of magnitude higher (Gupta *et al.*, 2016). In this case, maximum aeration efficiency was achieved under all conditions, as shown in Table 4. Whilst the pressure drop across the constriction is, within experimental error, the same for the three fluids, the relative increase in mean bubble size is greatest for fluid MF1 with the lowest PGE 55 content and reduces as the PGE 55 concentration increases for MF2 and MF3, as shown in Fig. 8.

Foams generated in the absence of a flow constriction have a relatively narrow BSD and have a peak at around 100 μm . Flow through the constriction, however, leads in all cases to a much broader positively skewed BSD. The effects are considerably more severe for fluid MF1 than MF2 and MF3. A possible reason for this may be due to the excess PGE 55 multilamellar vesicles available at higher concentrations to stabilise gas-liquid interfaces, clog plateau borders and thin films and, thus, slow down liquid drainage and inhibit film rupture and bubble coalescence (Jabarkhyl *et al.*, 2020a).

Duerr-Auster *et al.* (2008) who studied the effects of pH on the foamability of PGE 55 solutions inside a kitchen mixer, found that the adsorption kinetics of PGE 55 improved leading to much enhanced foamability when the pH was reduced from 7 to 3. They attributed this improvement to the partial destruction of PGE 55 multilamellar vesicles, thereby exposing a higher fraction of the hydrophobic bilayer core to the air-water interface. They also found that acidity increased the rate of bubble coalescence under static conditions by dramatically reducing coalescence time (Duerr-Auster *et al.*, 2008).

In this study, foams generated from fluid MF2 at pH 3 and pH 7 and G/L ratios of 1.0, 1.5 and 2.0 were allowed to flow through a short straight pipe with and without a 0.8 mm orifice plate fitted, but no significant effects were observed on either pressure drop or bubble size (data not shown). In this case, the improved adsorption kinetics of the PGE 55 surfactant was not sufficient to influence bubble coalescence during flow. Flow through the pipe with or without the constriction is relatively very fast and there is probably insufficient time for the diffusion of multilamellar vesicles of PGE 55 to have an effect.

3.4.3 Effects of xanthan gum concentration

The above flow experiments were repeated at G/L = 1.5 to study the effects of varying the concentration of xanthan gum using foams generated from fluids MF4, MF5 and MF2 containing respectively, 0.25, 0.35 and 0.50 wt% XG, but the same PGE 55 concentration (0.5 wt%). In this case, maximum aeration efficiency was achieved under all conditions, as shown in Table 5. Foams generated in the absence of a flow constriction have a relatively narrow BSD and have a peak at around 100 μm . Flow through the constriction, however, leads in all cases to a right shift in the BSDs which become much broader and positively skewed. The effects are most severe for fluid MF4. The pressure drop across the constriction

increases as a function of XG concentration, but the relative increase in mean bubble size is greatest for fluid MF4 with the lowest XG content and reduces as the XG concentration increases for MF5 and MF2, as shown in Fig. 9. The coarser foam texture at lower XG concentrations is probably due to the lower liquid viscosity causing weaker foam stability because of faster drainage, shorter thin liquid lifetime and higher rate of bubble coalescence.

3.4.4 Effects of rotor speed

Similarly, flow experiments were again performed at $G/L = 1.5$ but varying the rotor speed, viz $N = 500, 1000, 1500$ and 2000 rpm, using foams generated from fluid MF2. Maximum aeration efficiency was achieved at all conditions investigated as shown in Table 6. Increasing N over this range led to a modest increase in pressure drop across the constriction which can be explained by the finer foams generated (i.e. more complex thin liquid film network) which dissipate more energy in flow (Jabarkhyl *et al.*, 2020b). Flow through the constriction causes, in all cases, a considerable rise in the mean bubble size, as shown in Fig. 10. The relative increase in D_{32} , however, is lowest for $N = 2000$ rpm probably because of the much finer foam texture; in general, the finer the bubble size, the less the damage incurred through a constriction.

3.5 Foam elasticity and static stability

3.5.1 Foam elasticity

Oscillatory tests were performed in the linear viscoelastic region to probe the unperturbed foam structure. The storage modulus (G') is a function of air volume fraction and bubble size distribution. For very wet foams ($\phi < \sim 0.50$) bubble size distribution has negligible effects on (G') (Jabarkhyl *et al.*, 2020b). Typical G' measurements for foams generated from fluid MF2 at $G/L = 1.5$ and $N = 1000$ rpm are shown in Fig. 11. G' is the highest for foam generated under ambient condition since this foam has a very fine texture. In contrast, G' decreases as the pressure drop incurred across the orifice constriction increases, owing to the coarser texture of the emerging foam and the loss of air at the highest pressure drop shown (Table 3).

3.5.2 Foam drainage

The raw foams generated in the rotor-stator device are statically extremely stable at room temperature on a timescale of months (Jabarkhyl *et al.*, 2020a). To assess the effects of the interaction with the constriction on the foam static stability, 50 ml foam samples were collected at the outlet of the flow pipe with and without a constriction. The sealed samples were then stored at a controlled temperature of 50°C to enhance drainage and, consequently, shorten the foam lifetime and reduce experimental monitoring time. Typical foam drainage transients and foam half-life estimates for foams generated from fluid MF2 at $G/L = 1.5$ and $N = 1000$ rpm are shown in Fig. 12. Foams flowing in a short straight

pipe without incurring a significant pressure drop have a finer texture which provides more resistance to liquid flow and, hence, they exhibit the slowest drainage time and the longest half-life. In contrast, the half-life is significantly reduced for foams having passed through the orifice constriction which have a coarser texture and may also contain less air as a result (Table 3). Results show that the higher the pressure drop incurred, the less the foam stability.

4 Conclusions

Foams generated from viscous shear-thinning fluids in a continuous multi rotor-stator device exhibit long term static stability on the order of months due to their fine texture consisting of a uniform bubble size distribution and the high viscosity of their base liquid. Flow through a short straight pipe incurs a low pressure drop and produces no tangible effects on foam structure, thus, preserving the original bubble size and static stability of the foam. At low pressure drops, foams are able to squeeze through a narrow orifice constriction without incurring significant structural transformations. At higher pressure drops, flow through the constriction causes significant bubble coalescence and, in some cases, loss of air volume leading to much coarser and much less stable foam. Increased surfactant content, liquid viscosity and rotor speed reduce bubble coalescence and help preserve foam structure during dynamic interaction with a flow constriction.

Acknowledgements

Funding from EPSRC (Grant EP/N002075/1) and Unilever Colworth (UK) is gratefully acknowledged. Saifullah Jabarkhyl's PhD was funded by an EPSRC-Unilever studentship.

Notation

d	bubble diameter (m)
D_0	orifice plate diameter (m)
D_{32}	Sauter mean diameter (m)
$D_{32}^{(P_{atm})}$	Sauter mean diameter at atmospheric pressure (m)
$D_{32}^{(P)}$	Sauter mean diameter at pressure P (m)
F_{rel}	relative frequency (%)
G'	storage modulus (Pa)
G/L	ratio of volumetric flowrate of air to liquid (-)
MF1	model fluid 1
MF2	model fluid 2
MF3	model fluid 3
MF4	model fluid 4

471	MF5	model fluid 5
472	N	rotational speed (s^{-1})
473	p	level of statistical significance
474	ΔP_c	Pressure loss across constriction (Pa)
475	PGE 55	polyglycerol ester of fatty acid (-)
476	XG	xanthan gum (-)
477		
478	<i>Greek symbols</i>	
479	ϕ	air volume fraction (-)
480	ϕ_e	experimental air volume fraction (-)
481	ϕ_{th}^P	theoretical air volume fraction at pressure P (-)
482	ϕ_{th}^{Patm}	theoretical air volume fraction at atmospheric pressure (-)
483	$\dot{\gamma}$	shear rate (s^{-1})
484	τ	shear stress (Pa)
485	ρ	fluid density ($kg\ m^{-3}$)

487 References

- 488 BADVE, M. & BARIGOU, M. 2020. Local description of foam flow, deformation and pressure drop in
489 narrow constricted channels. *International Journal of Multiphase Flow*, 128, 103279.
- 490 BALERIN, C., AYMARD, P., DUCEPT, F., VASLIN, S. & CUVELIER, G. 2007. Effect of formulation and
491 processing factors on the properties of liquid food foams. *Journal of Food Engineering*, 78,
492 802-809.
- 493 BARIGOU, M. & DOUAIRE, M. 2013. 9 - X-ray micro-computed tomography for resolving food
494 microstructures. In: MORRIS, V. J. & GROVES, K. (eds.) *Food Microstructures*. Woodhead
495 Publishing.
- 496 CALVERT, J. R. 1988. The flow of foam through constrictions. *International Journal of Heat and Fluid*
497 *Flow*, 9, 69-73.
- 498 CALVERT, J. R. & NEZHATI, K. 1987. Bubble size effects in foams. *International Journal of Heat and*
499 *Fluid Flow*, 8, 102-106.
- 500 COX, A. R., ALDRED, D. L. & RUSSELL, A. B. 2009. Exceptional stability of food foams using class II
501 hydrophobin HFBII. *Food Hydrocolloids*, 23, 366-376.
- 502 CURSCHELLAS, C., KOHLBRECHER, J., GEUE, T., FISCHER, P., SCHMITT, B., ROUVET, M., WINDHAB, E. J.
503 & LIMBACH, H. J. 2013. Foams Stabilized by Multilamellar Polyglycerol Ester Self-Assemblies.
504 *Langmuir*, 29, 38-49.
- 505 CURSCHELLAS, C., NAGY, K., WINDHAB, E. & LIMBACH, H. J. 2013b. Characteristics of polyglycerol
506 ester and its different fractions. *Journal of Colloid and Interface Science*, 393, 182-191.
- 507 DESHPANDE, N. S. & BARIGOU, M. 2000. The flow of gas-liquid foams in vertical pipes. *Chemical*
508 *Engineering Science*, 55, 4297-4309.
- 509 DESHPANDE, N. S. & BARIGOU, M. 2001a. Foam flow phenomena in sudden expansions and
510 contractions. *International Journal of Multiphase Flow*, 27, 1463-1477.
- 511 DESHPANDE, N. S. & BARIGOU, M. 2001b. The flow of gas-liquid foams through pipe fittings.
512 *International Journal of Heat and Fluid Flow*, 22, 94-101.
- 513 DICKINSON, E. 2010. Food emulsions and foams: Stabilization by particles. *Current Opinion in Colloid*
514 *& Interface Science*, 15, 40-49.

- DICKINSON, E., ETTELAIE, R., MURRAY, B. S. & DU, Z. 2002. Kinetics of disproportionation of air bubbles beneath a planar air-water interface stabilized by food proteins. *J Colloid Interface Sci*, 252, 202-13.
- DUERR-AUSTER, N., EISELE, T., WEPF, R., GUNDE, R. & WINDHAB, E. J. 2008. Influence of pH on colloidal properties and surface activity of polyglycerol fatty acid ester vesicles. *Journal of Colloid and Interface Science*, 327, 446-450.
- DUERR-AUSTER, N., KOHLBRECHER, J., ZUERCHER, T., GUNDE, R., FISCHER, P. & WINDHAB, E. 2007. Microstructure and Stability of a Lamellar Liquid Crystalline and Gel Phase Formed by a Polyglycerol Ester Mixture in Dilute Aqueous Solution. *Langmuir*, 23, 12827-12834.
- ELLIS, A. L., NORTON, A. B., MILLS, T. B. & NORTON, I. T. 2017. Stabilisation of foams by agar gel particles. *Food Hydrocolloids*, 73, 222-228.
- GUPTA, M., HOOGHTEN, R. V., FISCHER, P., GUNES, D. Z. & VERMANT, J. 2016. Limiting coalescence by interfacial rheology: over-compressed polyglycerol ester layers. *Rheologica Acta*, 55, 537-546.
- HEUER, A., COX, A. R., SINGLETON, S., BARIGOU, M. & GINKEL, M.-V. 2007. Visualisation of foam microstructure when subject to pressure change. *Colloids and Surfaces A: Physicochemical and Engineering Aspects*, 311, 112-123.
- JABARKHYL, S., BARIGOU, M., BADVE, M. & ZHU, S. 2020b. Rheological properties of wet foams generated from viscous pseudoplastic fluids. *Innovative Food Science & Emerging Technologies*, 64, 102304.
- JABARKHYL, S., BARIGOU, M., ZHU, S., RAYMENT, P., LLOYD, D. M. & ROSSETTI, D. 2020a. Foams generated from viscous non-Newtonian shear-thinning liquids in a continuous multi rotor-stator device. *Innovative Food Science & Emerging Technologies*, 59, 102231.
- LIM, K. S. & BARIGOU, M. 2004. X-ray micro-computed tomography of cellular food products. *Food Research International*, 37, 1001-1012.
- MARY, G., MEZDOUR, S., DELAPLACE, G., LAUHON, R., CUVELIER, G. & DUCEPT, F. 2013. Modelling of the continuous foaming operation by dimensional analysis. *Chemical Engineering Research and Design*, 91, 2579-2586.
- MÜLLER-FISCHER, N., SUPPIGER, D. & WINDHAB, E. J. 2007b. Impact of static pressure and volumetric energy input on the microstructure of food foam whipped in a rotor-stator device. *Journal of Food Engineering*, 80, 306-316.
- MÜLLER-FISCHER, N. & WINDHAB, E. J. 2005. Influence of process parameters on microstructure of food foam whipped in a rotor-stator device within a wide static pressure range. *Colloids and Surfaces A: Physicochemical and Engineering Aspects*, 263, 353-362.
- MURRAY, B. S., DICKINSON, E., GRANSARD, C. & SÖDERBERG, I. 2006. Effect of thickeners on the coalescence of protein-stabilized air bubbles undergoing a pressure drop. *Food Hydrocolloids*, 20, 114-123.
- ZAYAS, J. F. 1997. Foaming Properties of Proteins. In: ZAYAS, J. F. (ed.) *Functionality of Proteins in Food*. Berlin, Heidelberg: Springer Berlin Heidelberg.

Table 1. Model fluids composition and properties.

Model fluid	PGE 55 (wt%)	XG (wt%)	Sugar (wt%)	ρ (kg m ⁻³)	σ_e (mN m ⁻¹)
MF1	0.2	0.50	25	1080	39
MF2	0.5	0.50	25	1080	38
MF3	1.0	0.50	25	1080	37
MF4	0.5	0.25	25	1080	38
MF5	0.5	0.35	25	1080	38

Table 2. Geometrical dimensions of continuous rotor-stator device.

Parameter	Symbol (unit)	Value
Diameter of annulus mixing space	L (mm)	5.00
Number of pins on rotor	I (-)	13.00
Number of rotor-stator pairs	h (-)	12.00
Distance between rotor-stator	s (mm)	1.00
Height of rotor/stator pin	q (mm)	2.50
Width of rotor pin	o (mm)	4.70
Rotor diameter	D (mm)	50.00
Distance between rotor pins	z (mm)	12.08

Table 3: Typical results of aeration efficiency and mean foam bubble size for different flow conditions obtained with fluid MF2 at $N = 1000$ rpm; $Q_L = 5.0$ L hr⁻¹; $Q_G^{(Patm)} = 5.0, 7.5$ and 10.0 L hr⁻¹. Values followed by different superscript letters in the same column are significantly different ($p < 0.05$).

Sample	ΔP_c (bar)	τ (s)	$D_{32}^{(P)}$ (μm)	$D_{32}^{(Patm)}$ (μm)	$\phi_{th}^{(P)}$ (-)	$\phi_{th}^{(Patm)}$ (-)	ϕ_e (-)	$\eta = \phi_e/\phi_{th}^{(Patm)}$ (-)
G/L = 1.0	No constriction	31	–	$147^h \pm 3$	0.500	0.500	0.500	1.00
$D_o = 1.8$ mm	0.047	32	$147^a \pm 3$	$157^g \pm 5$	0.477	0.500	0.500	1.00
$D_o = 0.8$ mm	0.300	38	$147^a \pm 5$	$200^f \pm 5$	0.385	0.500	0.500	1.00
$D_o = 0.6$ mm	0.880	45	$147^a \pm 7$	$230^e \pm 10$	0.266	0.500	0.500	1.00
$D_o = 0.5$ mm	1.450	49	$147^a \pm 13$	$323^c \pm 20$	0.204	0.500	0.460	0.92
G/L = 1.5	No constriction	25	–	$130^i \pm 3$	0.600	0.600	0.600	1.00
$D_o = 1.8$ mm	0.058	27	$130^b \pm 5$	$138^h \pm 5$	0.567	0.600	0.600	1.00
$D_o = 0.8$ mm	0.357	34	$130^b \pm 5$	$227^e \pm 10$	0.442	0.600	0.600	1.00
$D_o = 0.6$ mm	0.956	43	$130^b \pm 11$	$300^c \pm 20$	0.307	0.600	0.600	1.00
$D_o = 0.5$ mm	1.680	48	$130^b \pm 13$	$447^b \pm 50$	0.224	0.600	0.560	0.93
$D_o = 0.4$ mm	2.500	56	$130^b \pm 10$	$580^a \pm 50$	0.171	0.600	0.540	0.90
G/L = 2.0	No constriction	20	–	$113^j \pm 3$	0.670	0.670	0.670	1.00
$D_o = 1.8$ mm	0.069	23	$113^c \pm 5$	$127^i \pm 5$	0.627	0.670	0.670	1.00
$D_o = 0.8$ mm	0.417	32	$113^c \pm 5$	$251^d \pm 5$	0.473	0.670	0.670	1.00
$D_o = 0.6$ mm	1.120	42	$113^c \pm 13$	$320^c \pm 20$	0.316	0.670	0.640	0.96
$D_o = 0.5$ mm	1.790	47	$113^c \pm 10$	$590^a \pm 50$	0.236	0.670	0.610	0.91

Table 4: Effects of PGE 55 surfactant concentration on aeration efficiency and mean foam bubble size for fixed flow conditions at $N = 1000$ rpm; $Q_L = 5.0$ L hr⁻¹; $Q_G^{(Patm)} = 7.5$ L hr⁻¹. Values followed by different superscript letters in the same column are significantly different ($p < 0.05$).

Sample	ΔP_c (bar)	τ (s)	$D_{32}^{(P)}$ (μ m)	$D_{32}^{(Patm)}$ (μ m)	$\phi_{th}^{(P)}$ (-)	$\phi_{th}^{(Patm)}$ (-)	ϕ_e (-)	$\eta = \phi_e/\phi_{th}^{(Patm)}$ (-)
MF1; G/L = 1.5	No constriction	25	—	143 ^d ± 10	0.600	0.600	0.600	1.00
$D_o = 0.8$ mm	0.327	34	143 ^a ± 10	430 ^a ± 17	0.452	0.600	0.600	1.00
MF2; G/L = 1.5	No constriction	25	—	130 ^d ± 10	0.600	0.600	0.600	1.00
$D_o = 0.8$ mm	0.357	34	130 ^a ± 10	227 ^b ± 8	0.442	0.600	0.600	1.00
MF3; G/L = 1.5	No constriction	25	—	110 ^e ± 5	0.600	0.600	0.600	1.00
$D_o = 0.8$ mm	0.362	34	110 ^a ± 10	174 ^c ± 10	0.441	0.600	0.600	1.00

Table 5: Effects of XG concentration on aeration efficiency and mean foam bubble size for fixed flow conditions at $N = 1000$ rpm; $Q_L = 5.0$ L hr⁻¹; $Q_G^{(Patm)} = 7.5$ L hr⁻¹. Values followed by different superscript letters in the same column are significantly different ($p < 0.05$).

Sample	ΔP_c (bar)	τ (s)	$D_{32}^{(P)}$ (μ m)	$D_{32}^{(Patm)}$ (μ m)	$\phi_{th}^{(P)}$ (-)	$\phi_{th}^{(Patm)}$ (-)	ϕ_e (-)	$\eta = \phi_e/\phi_{th}^{(Patm)}$ (-)
MF4; G/L = 1.5	No constriction	25	-	150 ^d ± 10	0.600	0.600	0.600	1.00
$D_o = 0.8$ mm	0.256	32	150 ^a ± 10	338 ^a ± 10	0.478	0.600	0.600	1.00
MF5; G/L = 1.5	No constriction	25	-	140 ^d ± 10	0.600	0.600	0.600	1.00
$D_o = 0.8$ mm	0.300	33	140 ^a ± 10	300 ^b ± 10	0.462	0.600	0.600	1.00
MF2; G/L = 1.5	No constriction	25	-	130 ^d ± 3	0.600	0.600	0.600	1.00
$D_o = 0.8$ mm	0.357	34	130 ^a ± 10	227 ^c ± 10	0.442	0.600	0.600	1.00

Table 6: Effects of rotor speed (N) on aeration efficiency and mean foam bubble size for fixed flow conditions at G/L = 1.5; $Q_L = 5.0$ L hr⁻¹; $Q_G^{(Patm)} = 7.5$ L hr⁻¹. Values followed by different superscript letters in the same column are significantly different ($p < 0.05$).

Sample	ΔP_c (bar)	τ (s)	$D_{32}^{(P)}$ (μ m)	$D_{32}^{(Patm)}$ (μ m)	$\phi_{th}^{(P)}$ (-)	$\phi_{th}^{(Patm)}$ (-)	ϕ_e (-)	$\eta = \phi_e/\phi_{th}^{(Patm)}$ (-)
$N = 500$ rpm	No constriction	25	—	230 ^b ± 6	0.600	0.600	0.600	1.00
$D_o = 0.8$ mm	0.330	34	230 ^a ± 10	340 ^a ± 10	0.451	0.600	0.600	1.00
$N = 1000$ rpm	No constriction	25	—	130 ^d ± 5	0.600	0.600	0.600	1.00
$D_o = 0.8$ mm	0.357	34	130 ^b ± 10	227 ^b ± 10	0.442	0.600	0.600	1.00
$N = 1500$ rpm	No constriction	25	—	94 ^f ± 3	0.600	0.600	0.600	1.00
$D_o = 0.8$ mm	0.400	35	94 ^c ± 10	195 ^c ± 10	0.429	0.600	0.600	1.00
$N = 2000$ rpm	No constriction	25	—	77 ^g ± 3	0.600	0.600	0.600	1.00
$D_o = 0.8$ mm	0.432	36	77 ^c ± 10	122 ^e ± 10	0.420	0.600	0.600	1.00

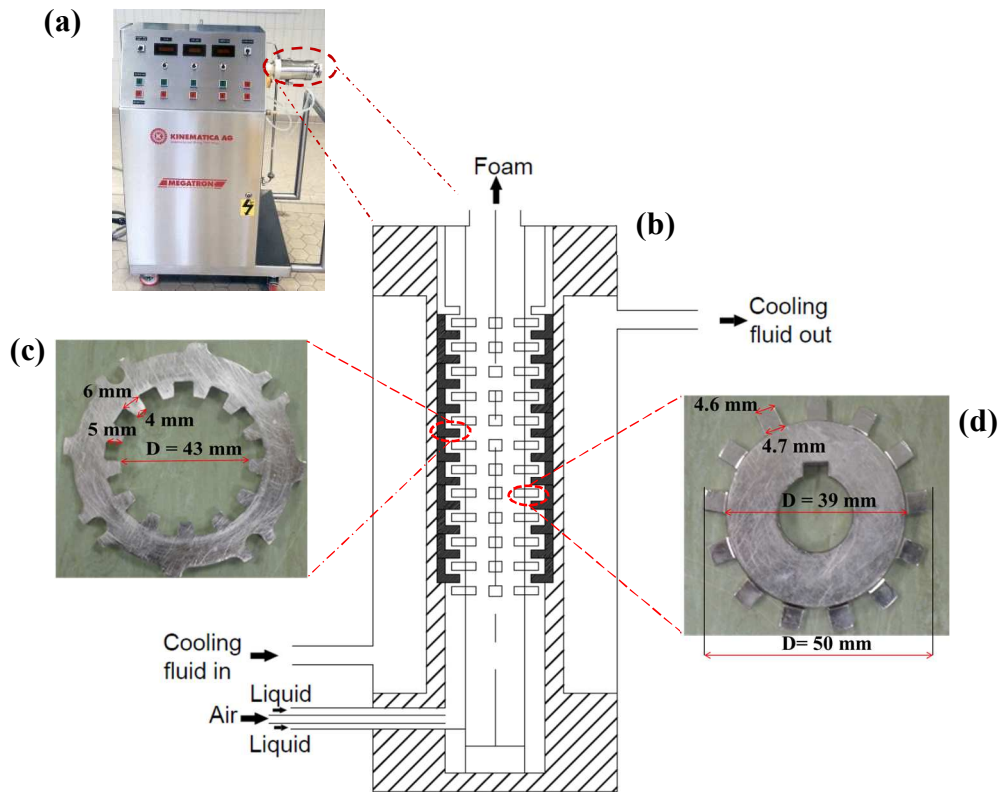


Fig. 1. Foam generator: (a) pilot-scale continuous rotor-stator unit; (b) schematic of mixing-head chamber; (c) stator; (d) rotor. The device consists of 12 rotor-stator pairs in series where, respectively, the rotor and stator have diameters of 50 and 52 mm each. Every rotor and stator has 13 pins ($4.7 \times 4.6 \times 2.5$ mm) with square ends and the gap between the rotor and stator is 1.0 mm.

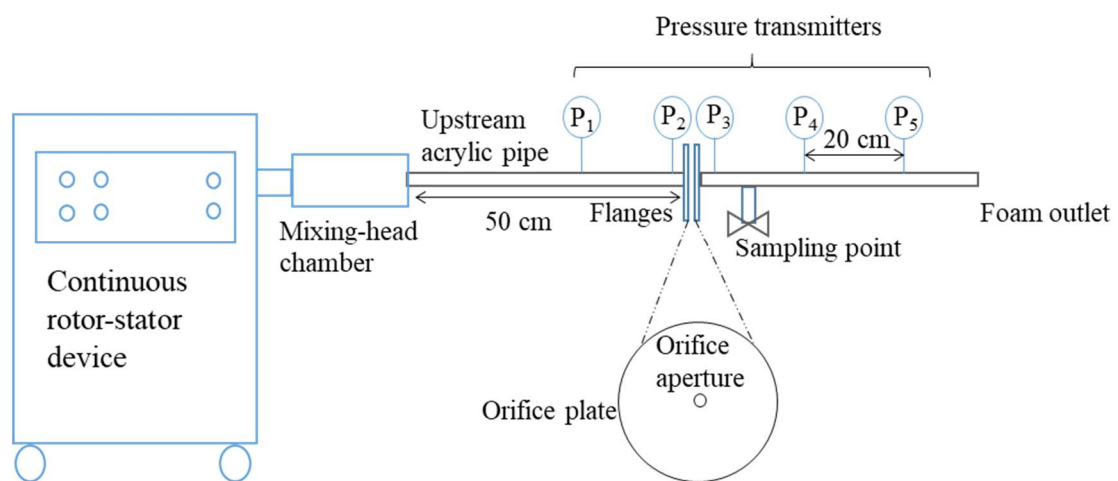


Fig. 2. Schematic of foam flow rig.

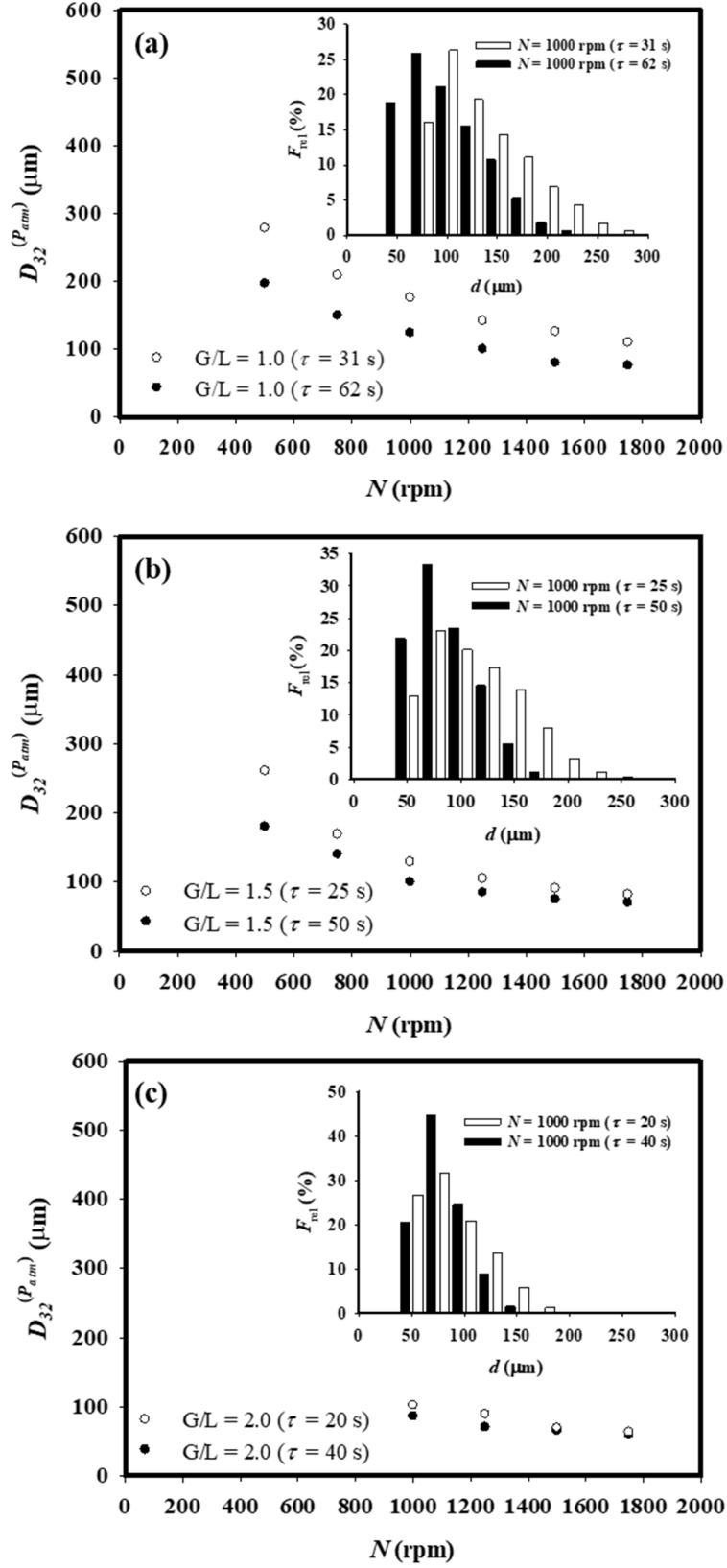


Fig. 3. Effects of residence time on bubble size of foams generated from fluid MF2: (a) $G/L = 1.0$ ($\phi_e = 0.52$); (b) $G/L = 1.5$ ($\phi_e = 0.62$); and (c) $G/L = 2.0$ ($\phi_e = 0.72$).

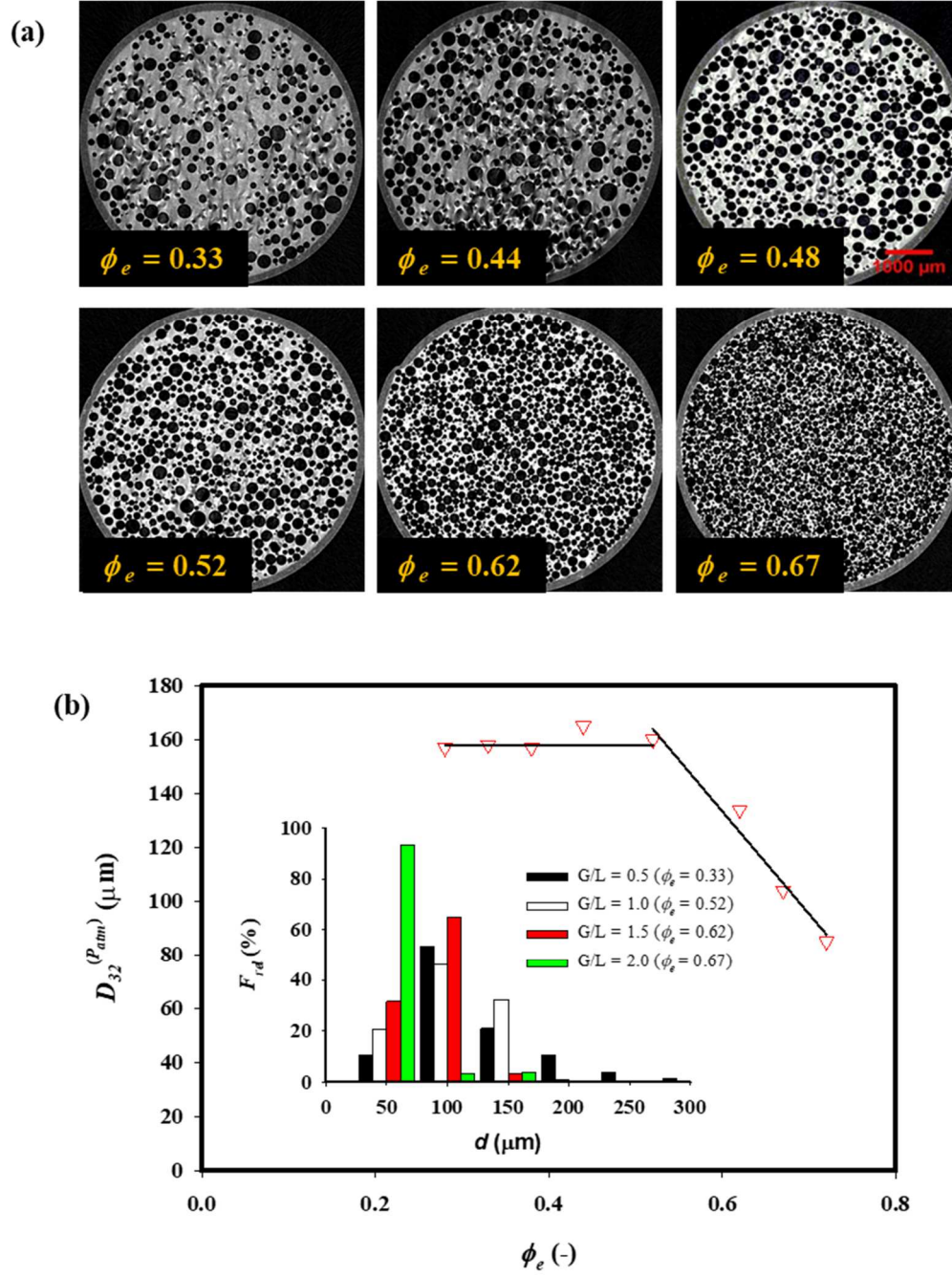


Fig. 4. Effects of air volume fraction on bubble size of foams generated from fluid MF2:
 $N = 1000$ rpm; $\tau = 40$ s.

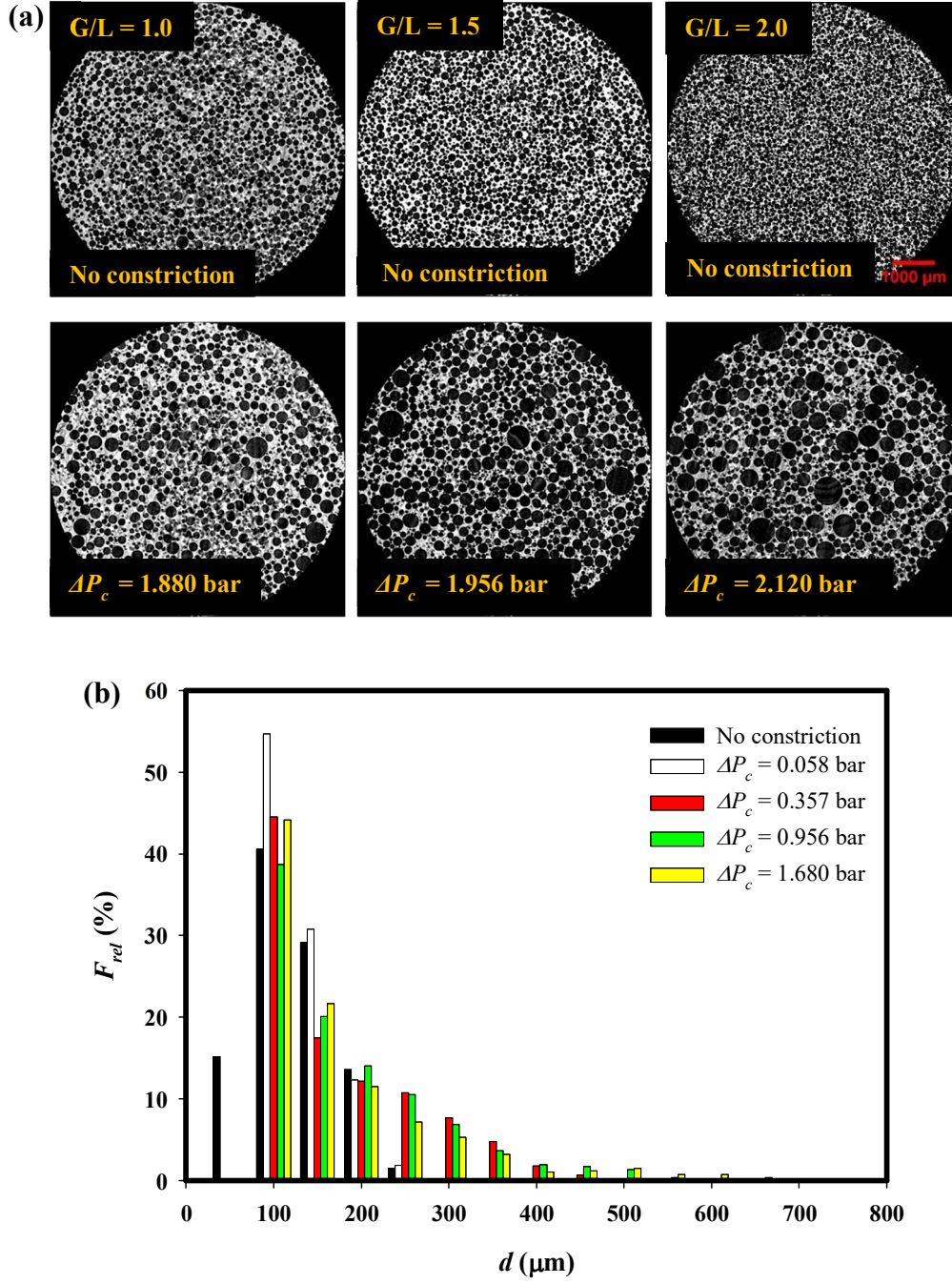


Fig. 5. Effects of pressure drop across constriction on foam microstructure generated from fluid MF2 at $N = 1000$ rpm, $G/L = 1.0$ ($\phi_{th}^{(P_{atm})} = 0.50$), $G/L = 1.5$ ($\phi_{th}^{(P_{atm})} = 0.60$), $G/L = 2.0$ ($\phi_{th}^{(P_{atm})} = 0.67$): (a) Typical X-ray micro-CT foam images; and (b) bubble size distributions.

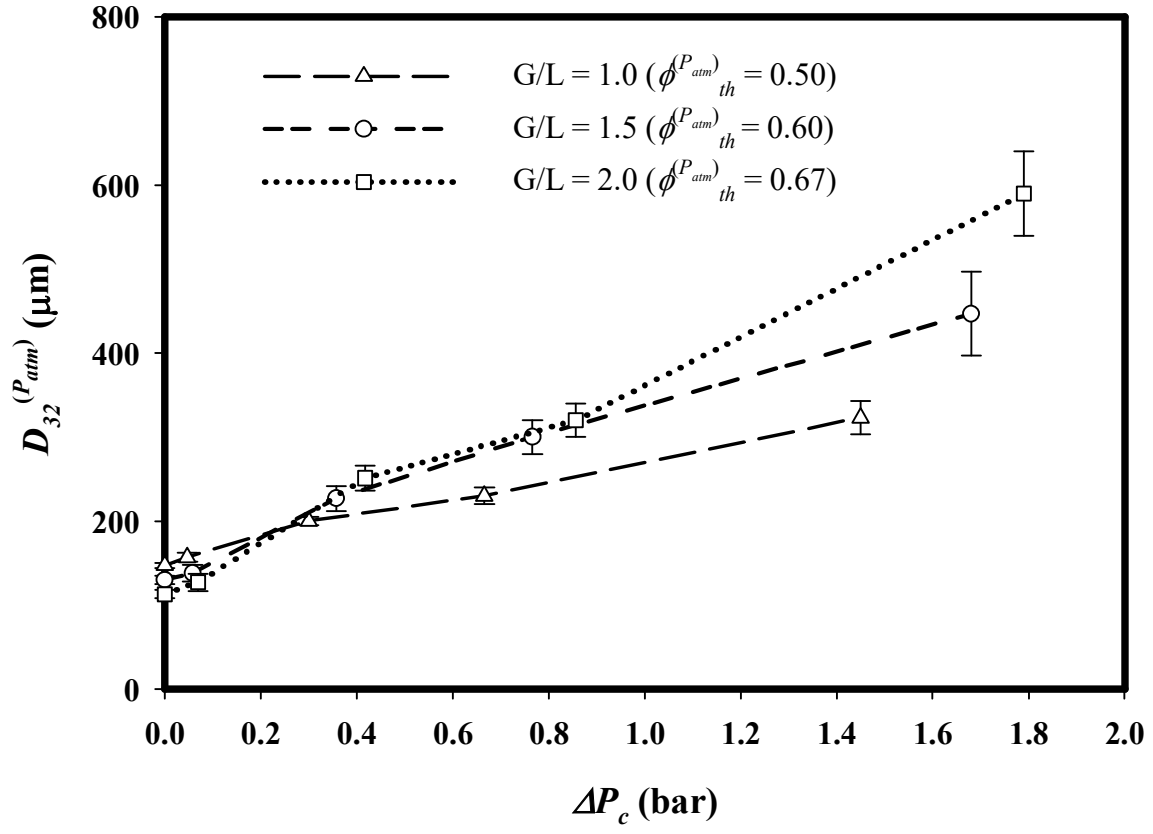


Fig. 6. Effects of pressure drop across constriction on mean bubble size of foams generated from fluid MF2 at $N = 1000$ rpm.

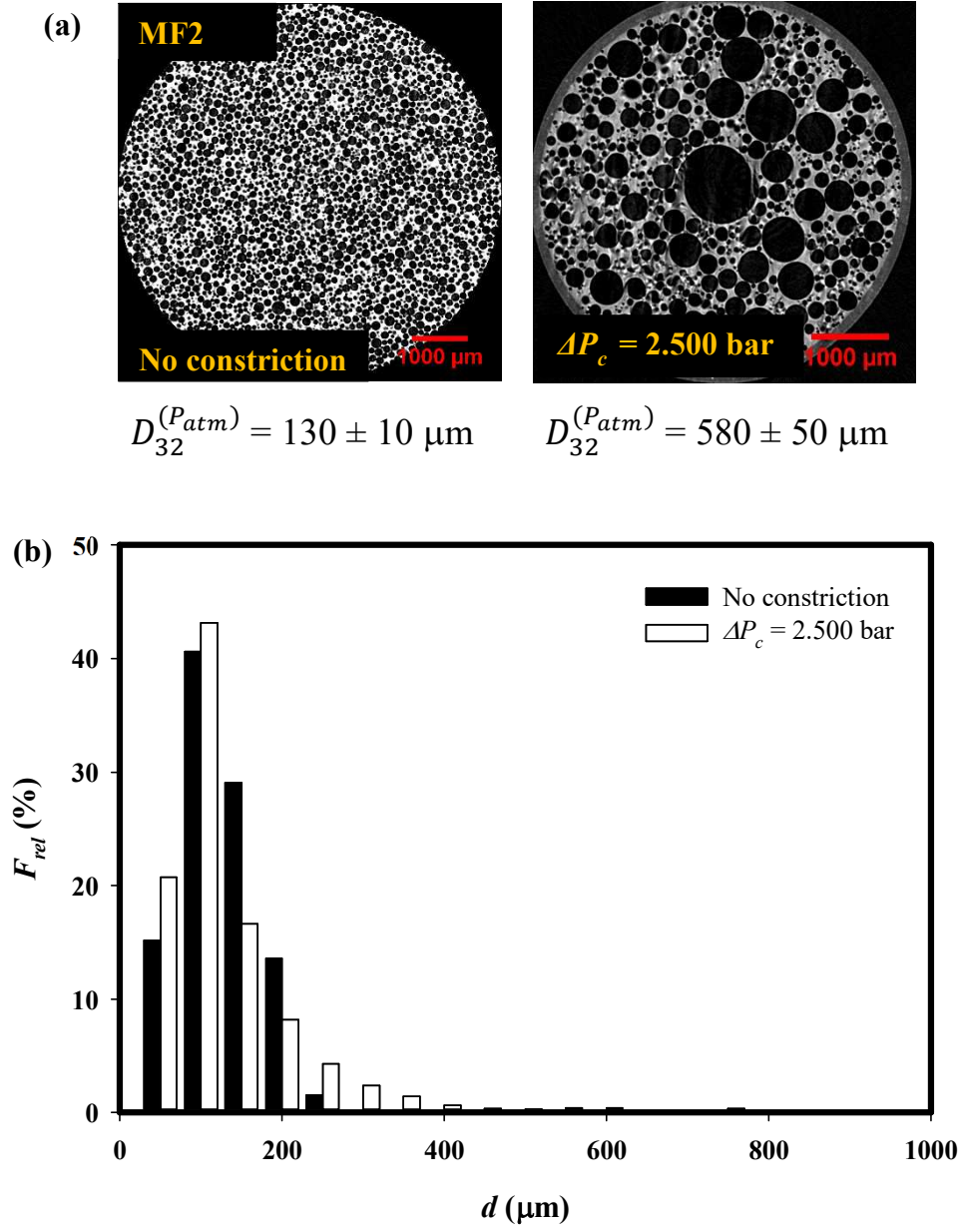


Fig. 7. Effects of pressure drop across constriction on bubble size of foams generated from MF2 at $N = 1000$ rpm, $G/L = 1.5$ ($\phi_{th}^{(P_{atm})} = 0.60$): (a) typical X-ray micro-CT foam images; and (b) bubble size distributions.

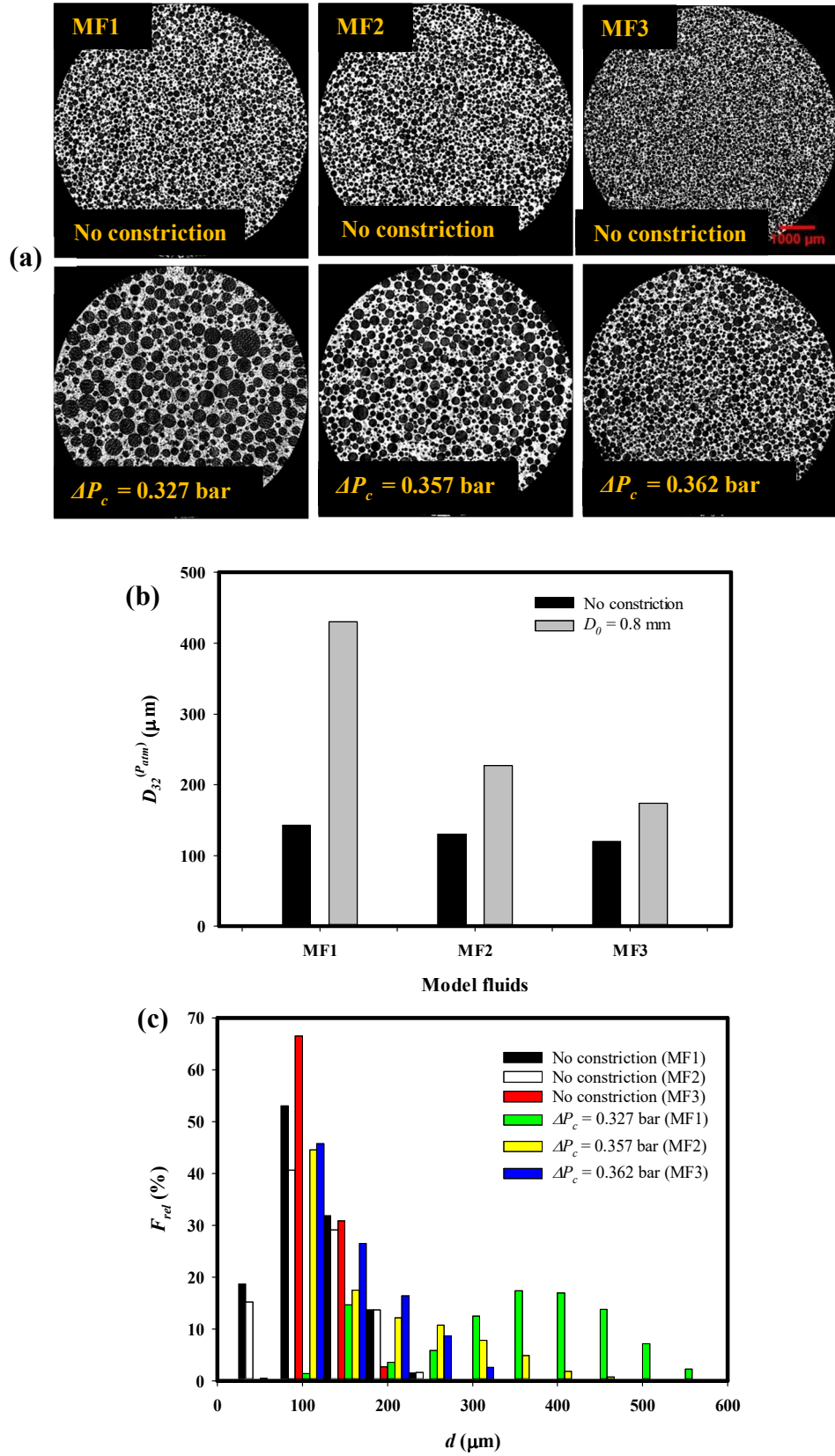


Fig. 8. Effects of PGE 55 concentration on bubble size of flowing foams generated from model fluids MF1 (0.2 wt%), MF2 (0.5 wt%) and MF3 (1.0 wt%) at $N = 1000$ rpm, $G/L = 1.5$ ($\phi_{th}^{(P_{atm})} = 0.60$): (a) X-ray micro-CT foam images; (b) mean bubble size variations; and (c) bubble size distributions.

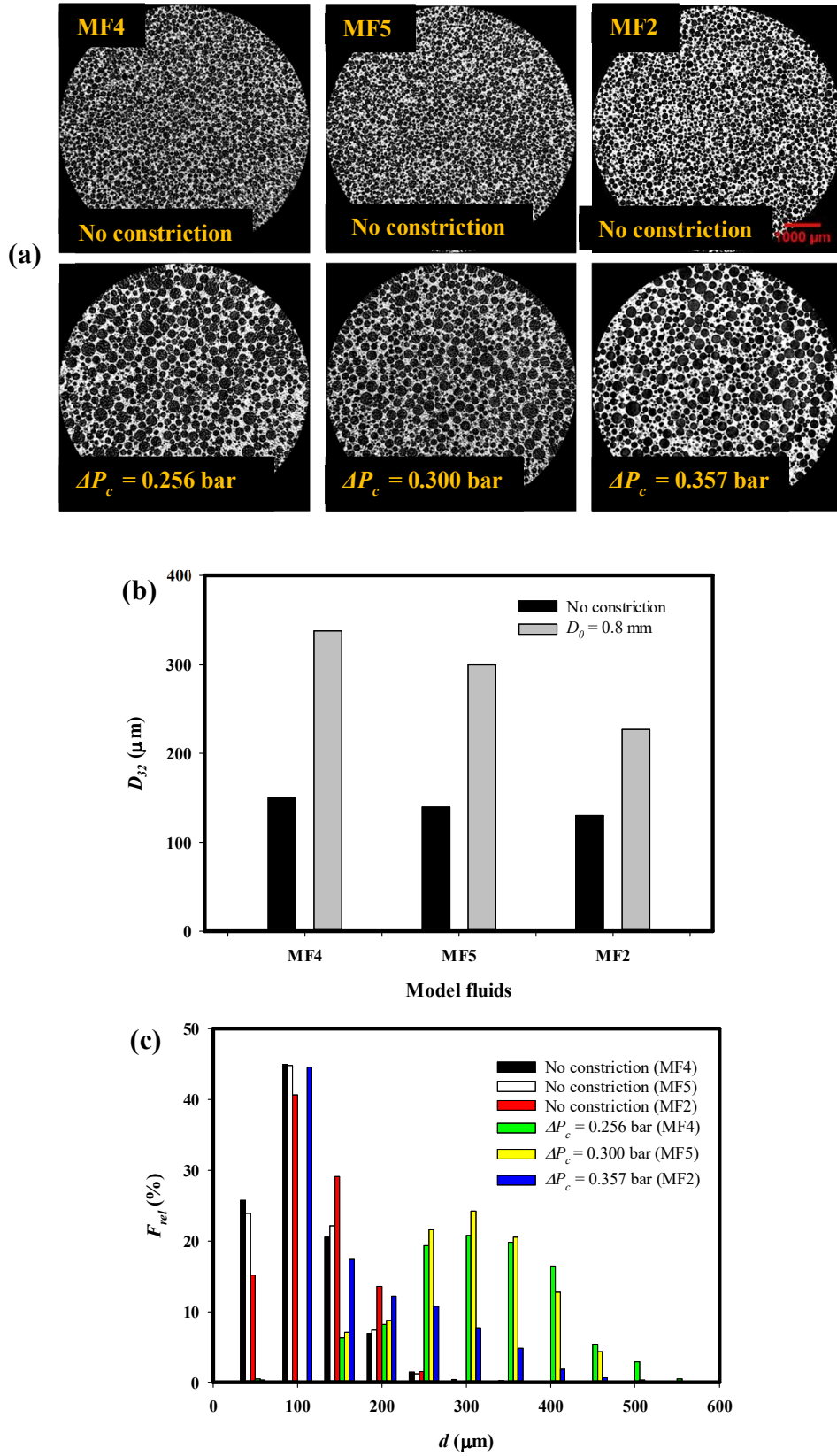


Fig. 9. Effects of xanthan gum concentration on bubble size of flowing foams generated from model fluids MF4 (0.25 wt%), MF5 (0.35 wt%) and MF2 (0.50 wt%) at $N = 1000$ rpm, $G/L = 1.5$ ($\phi_{th}^{(P_{atm})} = 0.60$): (a) X-ray micro-CT foam images; (b) mean bubble size variations; (c) bubble size distributions.

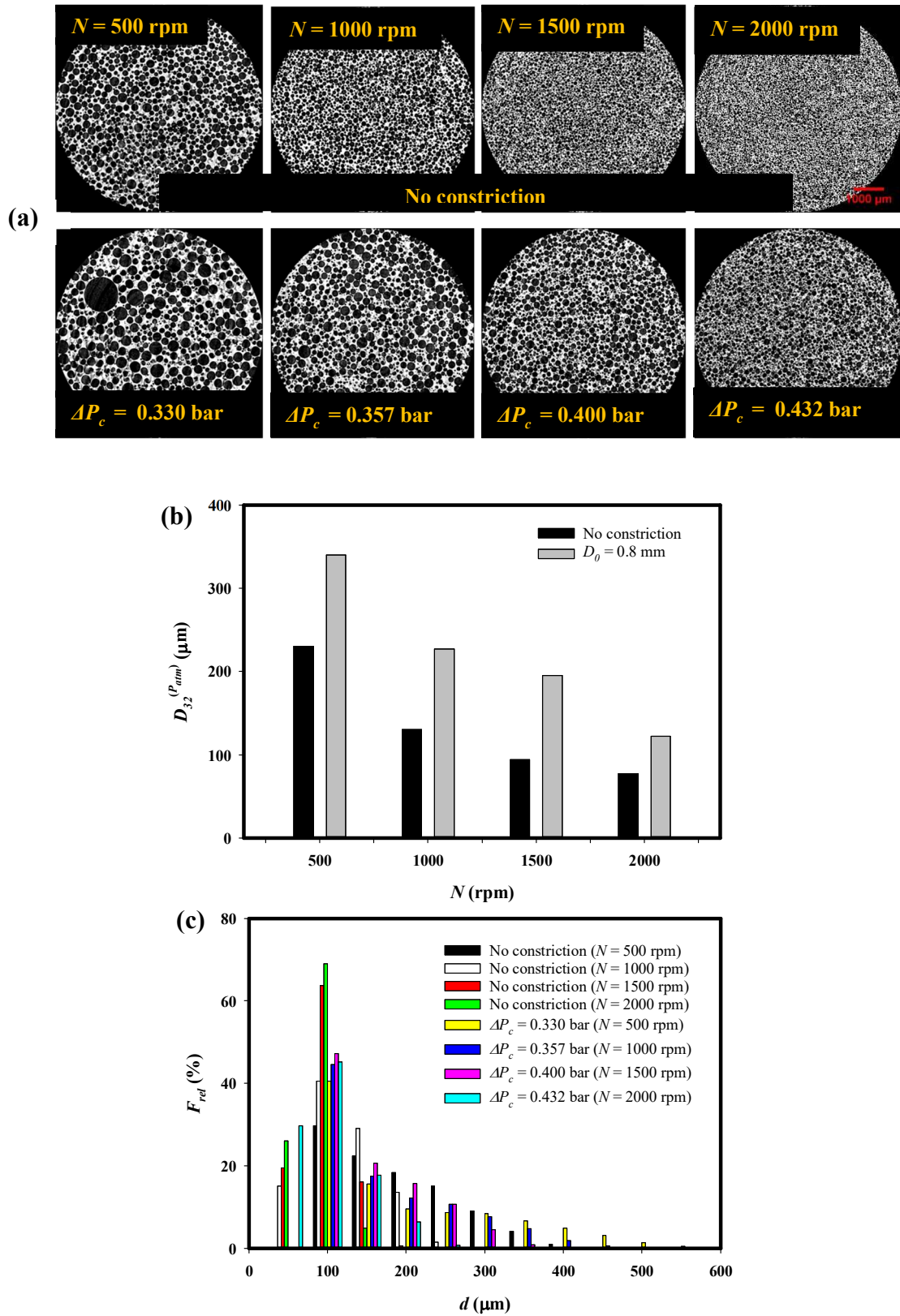


Fig. 10. Effects of rotor speed on bubble size of flowing foams generated from model fluids MF2 at $N = 500, 1000, 1500$ and 1750 rpm; $G/L = 1.5$ ($\phi_{th}^{(p_{atm})} = 0.60$): (a) X-ray micro-CT foam images; (b) mean bubble size variations; (c) bubble size distributions.

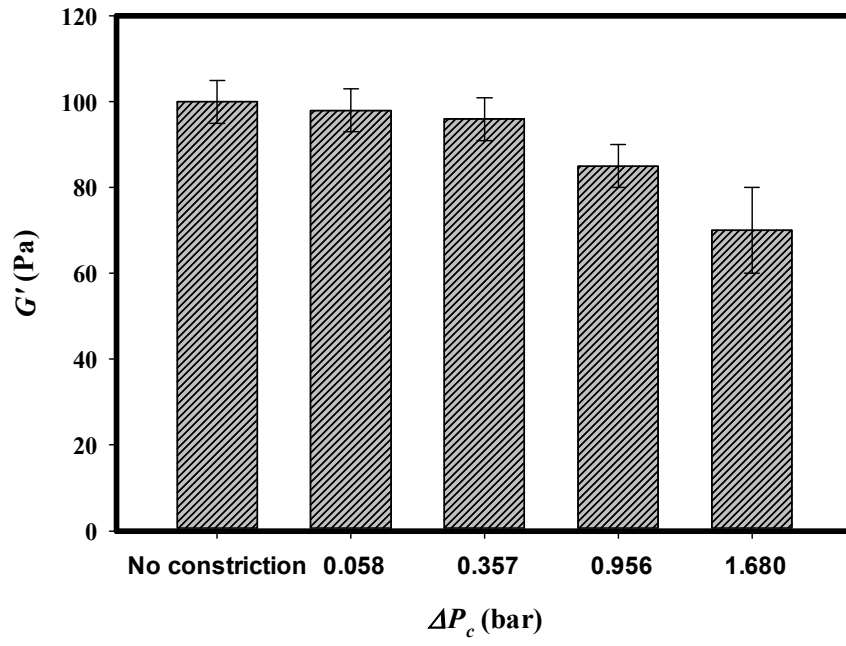


Fig. 11. Effects of pressure drop across constriction on elastic modulus of foam generated from fluid MF2:
 $N = 1000$ rpm, $G/L = 1.5$ ($\phi_{th}^{(P_{atm})} = 0.60$).

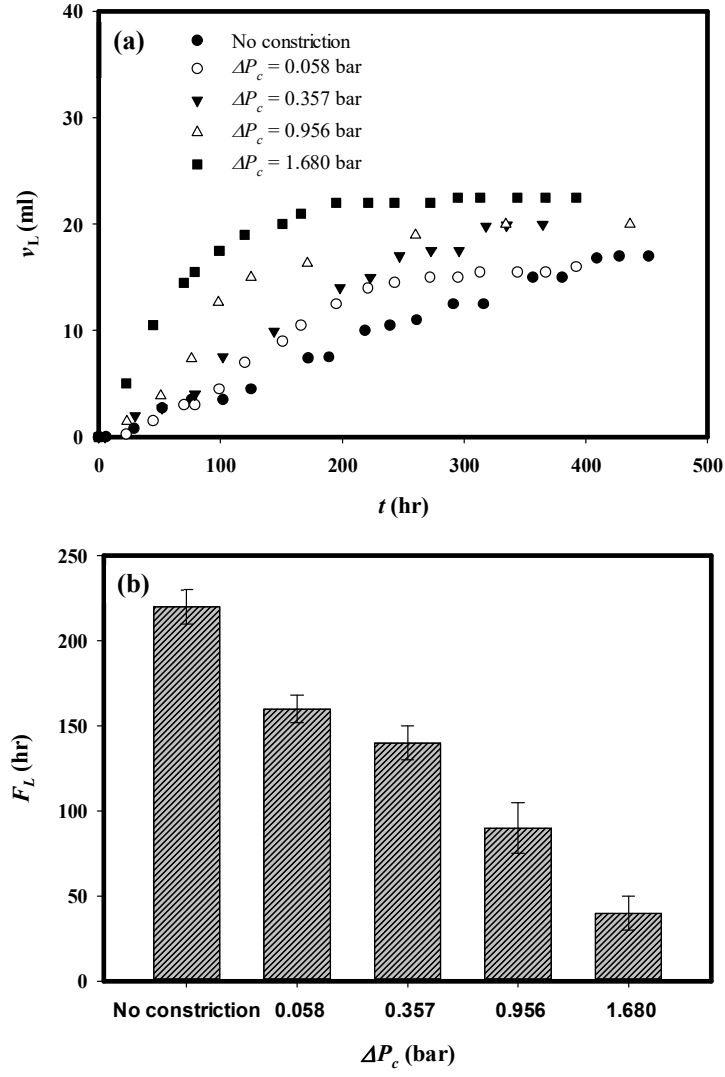


Fig. 12. Effects of pressure drop across constriction on drainage of foams generated from fluid MF2: $N = 1000$ rpm, $G/L = 1.5$ ($\phi_{th}^{(P_{atm})} = 0.60$): (a) foam drainage transient; (b) foam half-life.